

Discovery of Weyl semimetal TaAs

B. Q. Lv^{1,*}, H. M. Weng^{1,2,*}, B. B. Fu¹, X. P. Wang^{2,3,1}, H. Miao¹, J. Ma¹, P. Richard^{1,2}, X. C. Huang¹, L. X. Zhao¹, G. F. Chen^{1,2}, Z. Fang^{1,2}, X. Dai^{1,2}, T. Qian^{1,§}, and H. Ding^{1,2,§}

¹ *Beijing National Laboratory for Condensed Matter Physics and Institute of Physics, Chinese Academy of Sciences, Beijing 100190, China*

² *Collaborative Innovation Center of Quantum Matter, Beijing, China*

³ *Department of Physics, Tsinghua University, 100084, Beijing, China*

Abstract

Weyl semimetals are recently predicted class of materials that can be regarded as three-dimensional analogs of graphene breaking time reversal or inversion symmetry. Electrons in a Weyl semimetal behave as Weyl fermions, which have many exotic properties, such as chiral anomaly and magnetic monopoles in the crystal momentum space. The surface state of a Weyl semimetal displays pairs of entangled Fermi arcs at two opposite surfaces. However, the existence of Weyl semimetals has not yet been proved experimentally. Here we report the experimental realization of a Weyl semimetal in TaAs by observing Fermi arcs formed by its surface states using angle-resolved photoemission spectroscopy. Our first-principles calculations, matching remarkably well with the experimental results, further confirm that TaAs is a Weyl semimetal.

* These authors contributed equally to this work.

§ Corresponding authors E-mail: tqian@iphy.ac.cn, dingh@iphy.ac.cn

Although the subjects of high energy and condensed matter physics are very different, they sometimes share the same ideas. The most famous examples are the concepts of spontaneously broken symmetry and the Higgs mechanism. The emerging area of topological matter has borrowed some key concepts like Majorana fermions, which can be used to describe certain topological excitations in topological superconductors. Recently, the very important concept of chiral anomaly in quantum field theory describing Dirac and Weyl fermions has been applied to condensed matter systems (1-5). In high energy physics and field theory, Weyl fermions are three dimensions (3D) fermions with linear dispersion, which can be realized in realistic materials having crossing points of non-degenerate bands at the Fermi level (E_F) (Fig. 1A). These materials are called Weyl semimetals (WSM) (6-11).

The most interesting property of a Weyl fermion system is its chirality. The chiral anomaly, the non-conservation of the particle number under parallel electric and magnetic fields, will happen if a system contains only one type of Weyl fermions with a certain chirality (4-6). Due to the no-go theorem, the Weyl points in realistic materials must come in pairs with opposite chirality (12,13). However, these points can be moved to different momentum (k)-points, resulting in Weyl fermions with different chirality locating at different valleys in k space. Once separated from their partner in k -space, Weyl points are topologically stable because any perturbation respecting the translational symmetry can only shift but not annihilate them (14,15). Therefore, WSM can be viewed as a new type of topological non-trivial phase in condensed matter other than the Z_2 topological insulators (14-20), and may serve as a good platform for studying and manipulating novel topological quantum states.

A WSM has many exotic properties that can be divided into two groups. One is a set of abnormal transport properties including negative magneto-resistance, chiral magnetic effects and anomalous Hall effect (21-23). The other one is the unique topological surface states forming unclosed Fermi surfaces (FSs), called Fermi arcs (4,14,15). The appearance of a Fermi arc is determined from the bulk band structure, which contains Weyl points. Weyl points with positive (or negative) chirality will be projected to certain surfaces generating “source” (or “drain”) points for the Fermi arcs. Each Fermi arc must

start at a “source point” and end at a “drain point” (Fig 1B).

In this work, we report evidence from angle-resolved photoemission spectroscopy (ARPES) experiments for the existence of Fermi arcs on the surface of the newly proposed WSM material TaAs (14,15). Unlike most of the previously proposed WSM, the removal of the spin degeneracy of the bands are induced by the lack of inversion symmetry in the crystal structure rather than the breaking of the time reversal symmetry (4,7,24). The realization of the WSM phase in nonmagnetic materials allows direct observation of the Fermi arcs by ARPES because the complexity caused by a magnetic domain structure is absent here.

The crystal structure of TaAs (Fig. 1C), consisting of alternating stacking of Ta and As layers, is a NbAs type body-centered-tetragonal structure (25). The corresponding space group is $I4_1md$ and the lattice parameters are $a = b = 3.4348 \text{ \AA}$ and $c = 11.641 \text{ \AA}$. The adjacent TaAs layers are rotated by 90° and shifted by $a/2$. Due to the lack of inversion symmetry, first-principles calculations predict that TaAs is a time-reversal invariant 3D WSM with a dozen pairs of Weyl nodes in the Brillouin zone (BZ) (14,15). To prove this experimentally, we investigate the electronic structure of TaAs single crystals using ARPES. The core level spectrum in Fig. 1E shows the characteristic peaks of Ta and As elements, confirming the chemical composition of our TaAs samples. It is important to notice that the As $3d$ core levels have two sets of spin-orbital doublets, while the Ta $4f$ core levels have only one set of doublets, suggesting that the cleaved surface is As terminated. The cleaved (001) surfaces in our measurements are very flat at the millimeter scale (Figs. 1F and 1G), which is much larger than the $30 \times 20 \text{ \mu m}^2$ spot size of the incident light in our ARPES experiments. Consequently, a single surface domain can be measured by ARPES. High quality ARPES data of highly-dispersive and well-defined quasiparticle peaks (Fig. 1H) are obtained, enabling us to precisely determine the band structure and the Fermi surface (FS). As explained below, some fine features in the band structure and the FS are critical in our determination of a Weyl semimetal.

To investigate the electronic structure in the 3D BZ, we carried out photon energy dependent ARPES measurements. To our surprise, almost all the observed band dispersions do not show any noticeable change with varying the incident photon energy

over a wide range (20 – 400 eV) (some examples are shown in Figs. 2A-2E), indicating that they are non-dispersive along k_z . To understand the two-dimensionality of the experimental band structure, we carried out first-principles band structure calculations on (001) slabs with the As and Ta terminations, respectively (Figs. 2G and 2H). The experimental band dispersions are remarkably well reproduced by the calculated surface state (SS) band structure with the As termination, in agreement with the conclusion from our core level data. The reason for the absence of bulk bands can be understood in our calculations by the fact that the bulk bands have vanishing spectral weight within the topmost unit cell, where most of the surface-sensitive ARPES signal originates.

The removal of bulk bands in ARPES measurements enables us to compare directly the measured surface states and their FSs with the calculated results with great precision. The consistency between calculations and experiment is further confirmed by the overall electronic structure along the high-symmetry lines $\bar{M} - \bar{X} - \bar{\Gamma} - \bar{Y} - \bar{M} - \bar{\Gamma}$ in Figs. 2I-2K. As the four-fold symmetry is broken on the cleavage surface, the surface bands are predicted to be anisotropic along $\bar{\Gamma} - \bar{X}$ and $\bar{\Gamma} - \bar{Y}$. Indeed, such anisotropic features are clearly observed in our ARPES data (Fig. 2J). The excellent consistency between ARPES experiment and first-principles calculations provides us confidence in our FS assignments and in our conclusion of Weyl semimetal, since the calculations consist in bulk bands with Weyl points (14).

Another hallmark of a Weyl semimetal is the existence of Fermi arcs from surface states. The topological feature of the WSM only requires each Fermi arc to be started and ended at the surface projections of the Weyl points with opposite chirality. For systems with multiple pairs of Weyl points, the surface connection pattern is not uniquely determined by the bulk band structure and can be modified by changing the surface condition. On the TaAs (001) surface, there are the topologically nontrivial SS that form the Fermi arcs as well the normal SS that form the closed FS. The appearance of normal SS can generate complicated FS structure on the surface as shown in Fig. 4C. To figure out the detail connection pattern of the FS, one needs to analyze the ARPES data over the whole BZ together with the comparison to the theoretical results, which will be discussed in full detail in next paragraph. However, the proof for the existence of Fermi arcs can be

done with a relatively simple way, i. e., counting the times of FS crossing through an arbitrary closed loop in the surface BZ. It is obvious that each closed FS formed by the normal SS can only cross the reference loop even number of times. Only the unclosed Fermi arc can possibly cross the reference loop odd number of times. Therefore if we can find a specific reference loop containing totally odd number of FS crossing, then Fermi arcs must exist. This is a sufficient condition for the existence of Fermi arcs. For TaAs, we choose the reference loop to be $\bar{\Gamma}-\bar{X}-\bar{M}-\bar{\Gamma}$ as shown in Fig. 4A, which encloses three Weyl points predicted theoretically. Note that the Weyl point W1 is doubly degenerate as projected to the (001) surface BZ. There is no band crossing E_F along $\bar{\Gamma}-\bar{M}$ (Figs. 2I and 2J). Three bands are identified to cross E_F along $\bar{\Gamma}-\bar{X}$ at $k_x = 0.35, 0.44$ and $0.945 \pi/a$, respectively (Figs. 2A-2E). In Figs. 3B and 3C, two almost degenerate bands are identified to cross E_F at $k_y \sim 0.35 \pi/a$ along $\bar{X}-\bar{M}$. In addition, one feature near E_F is observed at $k_y \sim 0.12 \pi/a$ along $\bar{X}-\bar{M}$ in Figs. 3B and 3C, which arises from one electron-like band with the bottom just below E_F , in agreement with the calculations. Therefore, we identify that the surface FSs cross the closed route $\bar{\Gamma}-\bar{X}-\bar{M}-\bar{\Gamma}$ seven times with 3 times in $\bar{\Gamma}-\bar{X}$, 4 times in $\bar{X}-\bar{M}$ and zero time in $\bar{M}-\bar{\Gamma}$. This is a direct experimental evidence of the existence of Fermi arc in TaAs.

Next we show the Fermi arcs and their topology on the (001) surface of TaAs with the help of first-principles calculations in Fig. 4. The precise agreement with the experimental observation of the surface band structure gives us strong confidence in going beyond the resolution of the present ARPES experiment. A rough k -point sampling in the calculations gives an excellent reproduction of the surface FS in Fig. 4C. The extra fine k -point sampling calculations around the W2 and W1 Weyl points along both k_x and k_y directions are shown in Figs. 4D-4G. From the high-precision surface state calculations in Figs. 4D and 4E, there is one Fermi arc ($a1$) connecting W1 from W2 along the $\bar{\Gamma}-\bar{Y}$ direction. The arc $a5$, connecting the adjacent W1 points on either side of $\bar{\Gamma}-\bar{Y}$, is clearly identified in both experiment and calculations. In addition, one can see three additional arc-like lines ($a2, a3, a4$) connected to W1. $a2$ and $a4$ are also observed in our ARPES experiments but connect each other, thus determining their trivial nature. Based on the band structure in experiment and calculations (Figs. 4K-4M), we judge that $a3$ is

mainly a bulk state due to the finite-layer band structure calculations. The situation close to $\bar{\Gamma}-\bar{X}$ is similar, where we identify that $b1$ and $b5$ are non-trivial Fermi arc surface states.

In summary, we have observed Fermi arcs on the (001) surface of TaAs by using ARPES. The surface FS is identified to cross one-eighth of the (001) surface BZ an odd number of times, which gives a mathematically strong evidence of an odd number of Weyl points enclosed inside. The first-principles calculations have reproduced every detail of the experimental measurements, including the band dispersion and the surface Fermi surface. The shape of Fermi arcs and their connectivity are further identified and clearly shown for the first time. These confirm that we have discovered a Weyl semimetal in TaAs.

This work was supported by the Ministry of Science and Technology of China (No. 2013CB921700, No. 2015CB921300, No. 2011CBA00108, and No. 2011CBA001000), the National Natural Science Foundation of China (No. 11474340, No. 11422428, No. 11274362, and No. 11234014), and the Chinese Academy of Sciences (No. XDB07000000). The ARPES experiments were performed at the Dreamline of Shanghai Synchrotron Radiation Facility.

References

1. G. T. Volovik, JETP Lett. **75**, 55 (2002).
 2. Z. J. Wang *et al.*, Phys. Rev. B **85**, 195320 (2012).
 3. Z. J. Wang *et al.*, Phys. Rev. B **88**, 125427 (2013).
 4. G. Xu *et al.*, Phys. Rev. Lett. **107**, 186806 (2011).
 5. H. M. Weng *et al.*, MRS Bulletin **39**, 849 (2014).
 6. F. R. Klinkhamer, G. E. Volovik, Int. J. Mod. Phys. A **20**, 2795 (2005).
 7. X. G. Wan *et al.*, Phys. Rev. B **83**, 205101 (2011).
 8. A. A. Burkov, L. Balents, Phys. Rev. Lett. **107**, 127205 (2011).
 9. A. A. Burkov, M. D. Hook, L. Balents, Phys. Rev. B **84**, 235126 (2011).
 10. H. B. Nielsen, M. Ninomiya, Phys. Lett. B **130**, 389 (1983).
 11. L. Balents, Weyl electrons kiss. Physics **4**, 36 (2011).
 12. H. B. Nielsen, M. Ninomiya, Phys. B **185**, 20 (1981).
 13. H. B. Nielsen, M. Ninomiya, Nucl. Phys. B **193**, 173 (1981).
 14. Hongming Weng *et al.*, arXiv:1501.00060.
 15. Shin-Ming Huang *et al.*, arXiv:1501.00755.
 16. HaiJun Zhang *et al.*, Nat. Phys. **5**, 438–442 (2009).
 17. J. E. Moore, Nat. Phys. **5**, 378–380 (2009).
 18. D. Hsieh *et al.*, Nature **452**, 970–974 (2008).
 19. D. Hsieh *et al.*, Science **323**, 919–922 (2009).
 20. Y. Xia *et al.*, Nat. Phys. **5**, 398–402 (2009).
 21. A. A. Zyuzin, A. A. Burkov, Phys. Rev. B **86**, 115133 (2012).
 22. P. Hosur, X. L. Qi, Comptes Rendus Physique **14**, 857 (2013).
 23. S. A. Parameswaran *et al.*, Phys. Rev. X **4**, 031035 (2014).
 24. A. A. Burkov, L. Balents, Phys. Rev. Lett. **107**, 127205 (2011).
- S. Furuseth, K. Selte, A. Kjekshus, Acta. Chem. Scand. **19**, 95 (1965).

Fig. 1. Weyl semimetal and TaAs single crystal. (A) Three-dimensional Dirac-cone point (DCP) can be driven into Weyl nodes with opposite chirality by either time-reversal symmetry breaking (TRB) or inversion-symmetry breaking (ISB). (B) Weyl semimetal has Fermi arcs on its surface connecting projections of two Weyl points with opposite chirality. Weyl point is the magnetic monopole (MMP) in bulk momentum space. (C) Crystal structure of TaAs. The arrow indicates that the cleavage occurs between the As and Ta atomic layers, which produces two kinds of (001) surfaces with either As or Ta terminated atomic layers. (D) Bulk and projected (001) surface BZs with high-symmetry points indicated. (E) Core level photoemission spectrum measured at photon energy $h\nu = 70$ eV shows the characteristic As 3*d*, Ta 5*p* and Ta 4*f* peaks. (F) and (G) Pictures taken by metallographic microscope of cleaved sample surface of one TaAs crystal used in our ARPES measurements. (H) High quality ARPES spectra along $\bar{\Gamma} - \bar{X}$ show highly-dispersive and well-defined quasiparticle peaks.

Fig. 2. Electronic structures on the (001) surface BZ. (A)-(D) Intensity plots of second derivatives of ARPES data taken along $\bar{\Gamma} - \bar{X}$ at $h\nu = 30, 36, 42, 48$ eV, respectively. Dashed lines represent the extracted band dispersions. (E) Extracted band dispersions from the experimental data presented in (A)-(D). (F) Intensity plot of second derivatives of ARPES data at E_F along $\bar{\Gamma} - \bar{X}$ as a function of momentum and photon energy. The features at $k_x = 0.35, 0.44$ and $0.945 \pi/a$ indicate the momentum locations as the three surface state bands cross E_F . The feature at $k_x = 0.975 \pi/a$ is caused by the hole-like band, whose top nearly touches E_F . The photoemission intensities of the bands near $\bar{\Gamma}$ are strongly suppressed above 50 eV due to the matrix element effect, making the features at $k_x = 0.35$ and $0.44 \pi/a$ indiscernible. (G) Calculated band structure along $\bar{\Gamma} - \bar{X}$ in the (001) slab of a thickness of seven unit-cells with As and Ta terminated layers on each side. The intensity of red color scales the wave function spectral weight projected to the outmost one unit cell with the As termination. (H) Same as (G) but the spectral weight is projected to another side with the Ta termination. (I) and (J) Intensity plots of ARPES raw data and their second derivatives along the high-symmetry lines $\bar{M} - \bar{X} - \bar{\Gamma} - \bar{Y} - \bar{M} - \bar{\Gamma}$ on the (001) surface BZ, respectively. For comparison, the calculated bands with

considerable surface state components at the side of As termination are plotted on top of the experimental data in **(J)**. **(K)** Calculated band structure along $\bar{M}-\bar{X}-\bar{\Gamma}-\bar{Y}-\bar{M}-\bar{\Gamma}$. The red color indicates the bands with considerable wave function spectral weight projected to the outmost one unit cell on the As terminated surface, which reproduces well the experimental band structure.

Fig. 3. Photoemission intensity plot at E_F on the (001) surface BZ and band dispersions. **(A)** Photoemission intensity plot at E_F on the (001) surface BZ recorded at $h\nu = 54$ eV (outside the green box) and 36 eV (inside the green box). Black and red solid circles represent the Weyl points with opposite chirality in the (001) surface BZ. **(B)** and **(C)** Photoemission intensity map and energy distribution curves (EDCs) along $\bar{X}-\bar{M}$ ($C1$) indicated in **(A)**, respectively. **(D)** and **(E)** Same as **(B)** and **(C)**, respectively, but taken along $C2$. We identify two hole-like bands along $C2$, which are almost degenerate at $k_x = \pi/a$, confirming that the outer hole-like band along $C1$ are doubly degenerate. **(F)** and **(G)** Photoemission intensity plot and momentum distribution curves (MDCs) along $C3$, respectively, show that two hole-like bands cross E_F . **(H)** and **(I)** Same as **(B)** and **(C)**, respectively, but taken along $\bar{Y}-\bar{M}$ ($C4$) show that two hole-like bands cross E_F . For comparison, the calculated surface state bands along $\bar{X}-\bar{M}$ and $\bar{Y}-\bar{M}$ are plotted on top of the experimental data in **(B)** and **(H)**, respectively. The dashed lines in **(E)**, **(G)** and **(I)** track the band dispersions.

Fig. 4. Identification of surface state Fermi arcs in TaAs. **(A)** Blue circles indicate the momentum locations as the surface state bands cross E_F along the close route $\bar{\Gamma}-\bar{X}-\bar{M}-\bar{\Gamma}$. Yellow and red circles represent the Weyl points with opposite chirality. **(B)** Photoemission intensity plot at E_F around W1 shows the experimental observation of one Fermi arc, corresponding to $a5$ in **(E)**. **(C)** Rough k -point sampling calculations of surface states at E_F distributed in the (001) surface BZ. **(D)-(G)** Fine k -point sampling calculations of surface states at E_F near the Weyl points. The Weyl point W1 is indicated as circles in **(E)** and **(F)** because the chemical potential in the calculations deviate slightly from the energy of W1. In **(E)** and **(F)** $a1-a5$ and $b1-b5$ represent the arc-like lines

connecting to W1 nearby $\bar{\Gamma}-\bar{Y}$ and $\bar{\Gamma}-\bar{X}$, respectively. The red arrows indicate the identified non-trivial Fermi arcs. **(H)-(J)** EDCs, intensity plot and calculated surface state bands along $C5$, respectively, show that two surface state bands cross E_F , forming $a1$ and $a2$, respectively. **(K)-(M)** Same as **(H)-(J)**, respectively, but taken along $\bar{\Gamma}-\bar{X}$, show that two surface state bands cross E_F , forming $b4$ and $b5$, respectively. The $a3$ and $b3$ are from the bulk states with some spectral weight on the surface due to finite-layer slab calculations.

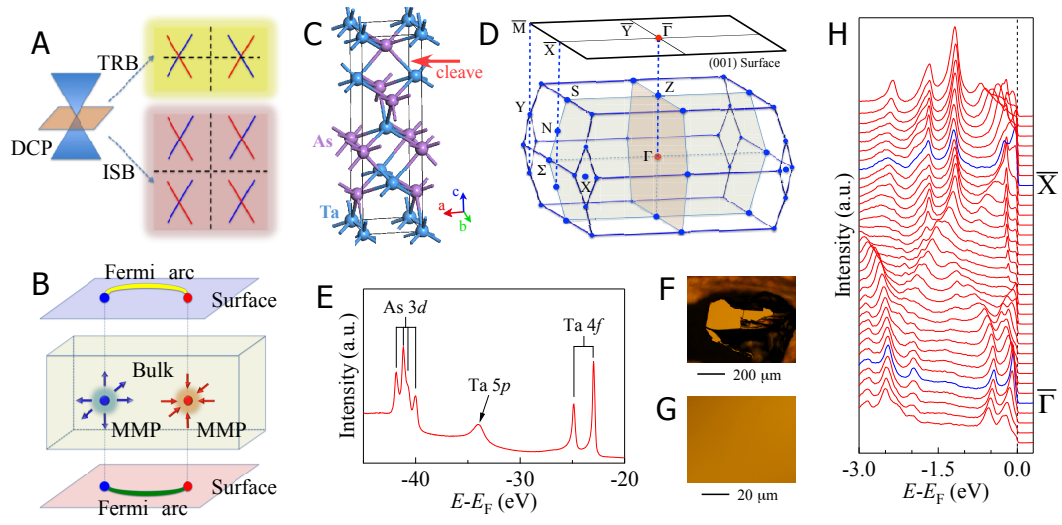


Fig. 1

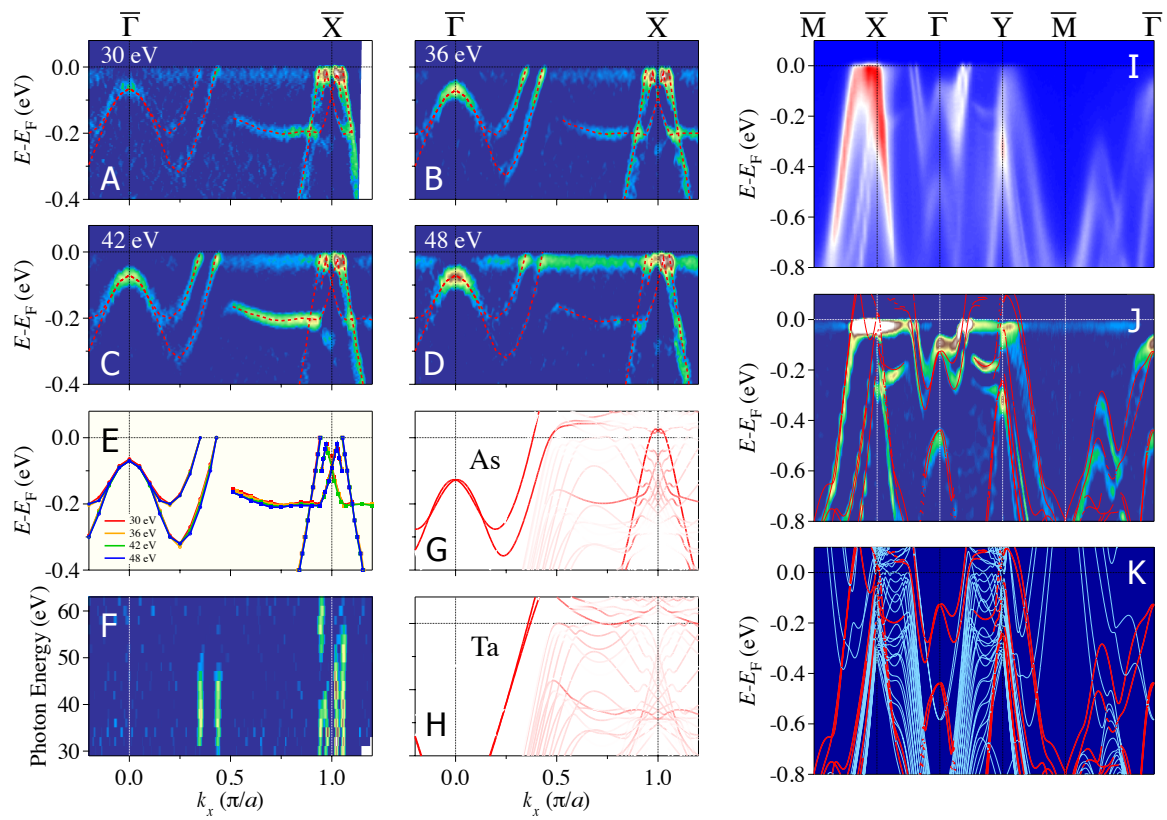


Fig. 2

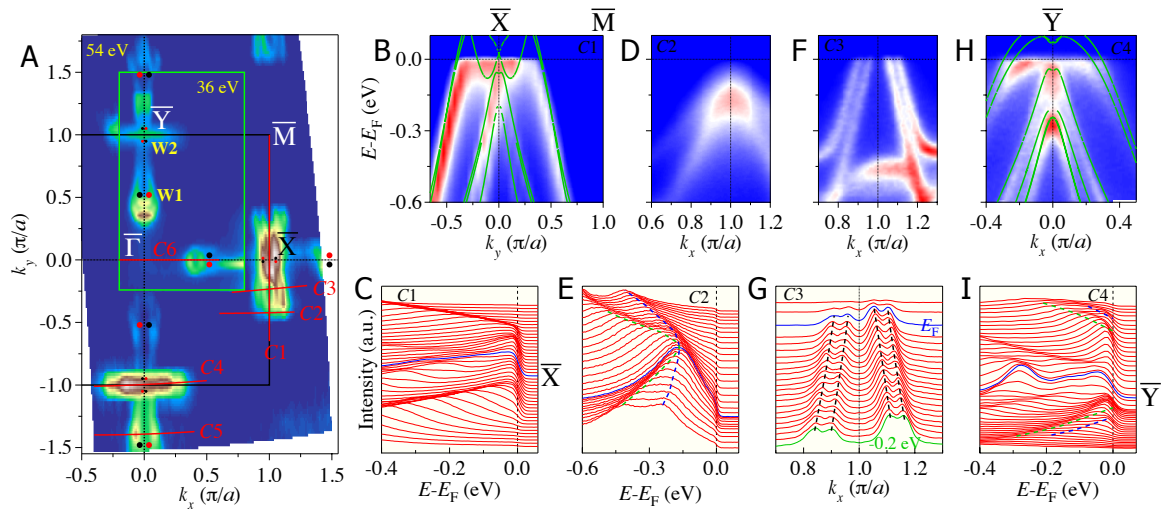


Fig. 3

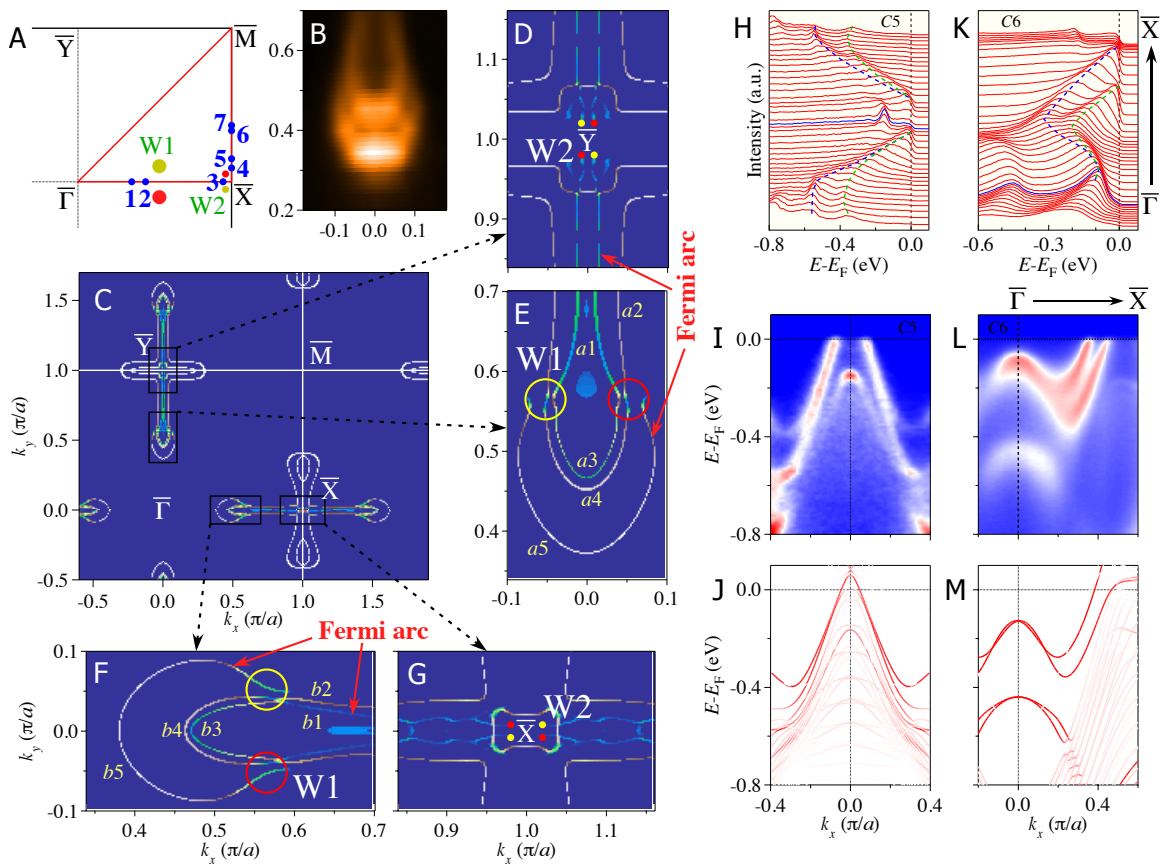


Fig. 4